Additively-manufactured PEEK/HA porous scaffolds with highly-controllable mechanical properties and excellent osteogenesis for bone tissue repairing

Jibao Zheng[1#], Huiyu Zhao[2#], Enchun Dong[1], Jianfeng Kang[3], Chaozong Liu[4], Changning Sun[1], Dichen Li[1*], Ling Wang[1*]

[1] *State Key Laboratory for Manufacturing System Engineering, School of Mechanical Engineering, Xi'an Jiaotong University, Xi'an, 710054, Shaanxi, China.*

[2] *Academy of Orthopedics, Guangdong Province, Orthopaedic Hospital of Guangdong Province, The Third Affiliated Hospital of Southern Medical University, Guangzhou 510665, People's Republic of China.*

[3] *Jihua Laboratory, Foshan, 528200, Guangdong, China.*

[4] *John Scale Centre for Biomedical Engineering, University College London, Royal National Orthopaedic Hospital, Stanmore HA7 4LP, UK*

Jibao Zheng and Huiyu Zhao are co-first authors of the article.

*Corresponding authors:

Dichen Li

Email: xjtudcli@sina.com

Address: State Key Laboratory for Manufacturing Systems Engineering
Xi'an Jiaotong University, Xi'an 710054, Shaanxi, China

Ling Wang

Email: menlwang@xjtu.edu.cn

Address: State Key Laboratory for Manufacturing Systems Engineering
Xi'an Jiaotong University, Xi'an 710054, Shaanxi, China

Abstract

Polyetheretherketone (PEEK) was widely applied into fabricating of orthopedic implants, benefitting its excellent biocompatibility and similar mechanical properties to native bones. However, the inertness of PEEK hinders its integration with the surrounding bone tissue. Here PEEK scaffolds with a series of hydroxyapatite (HA) contents in gradient were manufactured via fused filament fabrication (FFF) 3D printing techniques. The influence of the pore size, HA content and printing direction on the mechanical properties of the PEEK/HA scaffolds was systematically evaluated. By adjusting the pore size and HA contents, the elastic modulus of the PEEK/HA scaffolds can be widely tuned in the range of 624.7-50.6 MPa, similar to the variation range of natural cancellous bone. Meanwhile, the scaffolds exhibited higher Young's modulus and lower compressive strength along Z printing direction. The mapping relationship among geometric parameters, HA content, printing direction and mechanical properties was established, which gave more accurate predictions and controllability of the modulus and strength of scaffolds. The PEEK/HA scaffolds with the micro-structured surface could promote cell attachment and mineralization *in vitro*. Therefore, the FFF-printed PEEK/HA composites scaffolds can be a good candidate for bone grafting and tissue engineering.

Keywords: Polyether-ether-ketone (PEEK); Scaffold; Composites; Fused filament fabrication (FFF); Mechanical properties

1. Introduction

Porous scaffold has been widely used in tissue engineering to provide appropriate environment and architecture for the regeneration of tissue[1-3]. Compared with conventional preparation techniques of scaffold, 3D printing techniques exhibit attractive attention for constructing controllable macro/microarchitectures[4, 5] , such as the porosity, the pore size, the pore shape and the interconnected network[6]. Thus, 3D printing techniques simplifies the fabrication process and provides more effective manufacturing method for the porous scaffolds. To date, the 3D printing metallic porous scaffold made from nickel[7], cobalt-chromium[8], titanium alloys[9, 10] and stainless steel[11] have been widely developed and applied in medicine fields. But the mechanical properties of the metallic scaffolds are quite different from those of natural bone, which lead to stress shielding and prosthetic loosening in the long term.

In recent years, high molecular polymers such as polylactic acid[12, 13], polycaprolactone[14] and polyetheretherketone (PEEK) were widely used in the tissue engineering for their excellent mechanical properties and biocompatibility. PEEK has been applied into fabricating porous scaffold structures. Su[15] et al. fabricated PEEK scaffolds by fused filament fabrication (FFF) process and *in vivo* experiments demonstrated that the newly-regenerated soft tissues could grow into the scaffold quickly. However, the soft tissue cannot adhere closely to the surface of the PEEK scaffolds ascribing to the biological inertness. Ahn[16] et al. fabricated PEEK scaffold by salt leaching method and the animal experiment results showed that the pure PEEK exhibited lower osteogenesis ability and interfacial strength. Thus, biological inertness and poor osteogenic capability restrict the clinical application of PEEK. Numerous studies were conducted to enhance the bioactivity of PEEK via the incorporation of additives such as hydroxyapatite (HA), calcium phosphate (TCP), bioglass (BGA).

Zhao[17] et al. prepared HA/PEEK composite by mixing hydroxyapatite and PEEK, finding that the composite promote osteoblastic cell adhesion and expression of bone-building protein. Rui Ma[18] et al. synthesized PEEK/CS composites, of which the hydrophilicity, alkaline phosphatase activity, and the mineralized nodule formation of composite were dramatically improved. But the study in 3D printing PEEK-based composite porous scaffolds was rare because of the complicated fabrication procedure.

In addition to the bioactivity, the mechanical properties of the scaffolds significantly affect the load transmitting and tissue growth[19-22]. The micro-structure of the scaffolds such as pore architecture[23, 24], pore size[25] and porosity[26, 27], impacted the mechanical performances of the scaffold greatly. Liang[28] et al. fabricated square, hexagonal and wheel-shaped porous scaffolds by 3D printing, finding that the square scaffolds exhibited better mechanical strength and fatigue properties. Melchels[29]et al. fabricated PLA scaffolds and found that effective modulus of the scaffolds with cube architecture was twice larger than those of gyroid architecture (324±39 MPa vs 169±21 MPa). Bagheri[30] et al. controlled the Young's modulus of the PLA scaffolds in the range of 250-700 MPa by changing the width of the struts. Thus the mechanical properties of scaffold could be controlled to a certain extent by changing the micro-architectures. However, the influences of the printing direction and the material components on the mechanical properties of the PEEK-based scaffold is still unclear.

In this study, PEEK/HA composites scaffolds with different pore size and HA content were fabricated via FFF 3D printing technology. The surface microstructure, surface roughness and internal architectures of PEEK/HA porous scaffolds were measured. The thermal analysis measurements of the PEEK composites were carried out to evaluate the crystalline and thermal behaviors. The influences of the micro-structure, HA content and printing direction on the mechanical properties of the PEEK/HA scaffolds was systematically investigated. Meanwhile, high-speed camera was used to record the compressive deformation process of the composite scaffolds to analyze the deformation mechanism. Finally, Cell culture experiments were performed to investigate the biocompatibility and mineralization *in vitro*.

2. Materials and methods

2.1 Fabrication of PEEK/HA composite scaffolds

The fabrication schematic of the scaffolds via FFF 3D printing process was shown as Figure 1. PEEK (50 μm) and HA (15 μm) powder were mixed with mass ratio of 8:2 and 6:4. Then the mixing composites was fed into a twin-screw extruder, from which they were extruded into filaments with a diameter of 1.75 mm. Tetragonal scaffold samples (length, width and thickness of 10 mm) were fabricated by based FFF process. The basic printing parameters were set as follows: nozzle temperature of 420 °C, layer thickness of 0.2mm, bead width of 0.4 mm and printing speed of 30 mm/s.

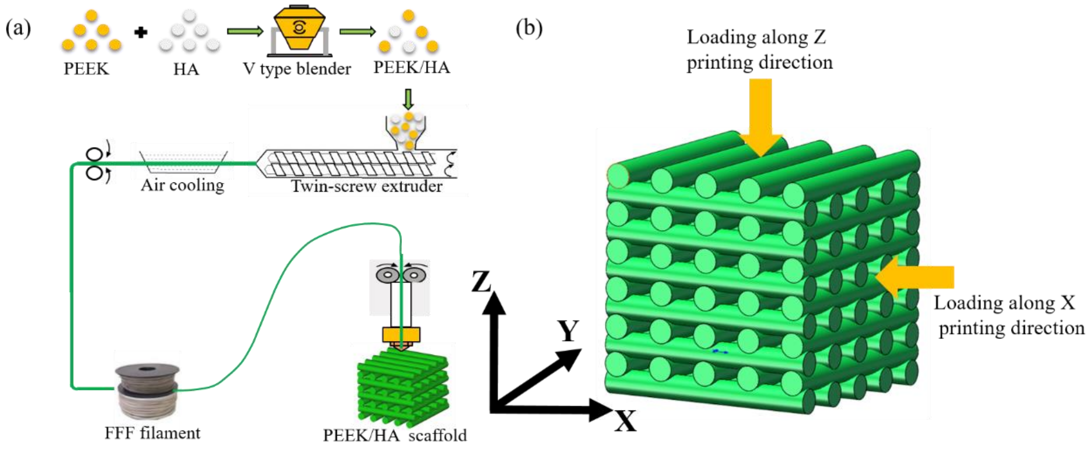

Figure 1. Schematic illustration of the 3D printing process and mechanical properties testing method: (a) preparation of PEEK/HA composites and FFF printing (b) scaffold compressed along Z or X printing direction.

2.2 Characteristics of the composite scaffolds

The structures of the composites scaffolds were measured using a micro computed tomography (Micro-CT, Y.Cheetah, YXLON, Germany) and reconstructed by the software of VG Studio Max 3.0. The surface morphologies of the scaffolds were characterized via scanning electron microscopy (SEM, su-8010, Hitachi, Japan) at an acceleration voltage of 5 kV after coated with a thin layer of Au. PEEK/HA scaffolds were observed on a laser scanning confocal microscope (LSCM, OLS4000, Olympus, Japan) to evaluate the surface roughness (*Ra*).

2.3 Thermal behaviors of the composites

Changes in chemical bonds was measured by Fourier Transform Infrared (FTIR, Nicolet iS10, Thermo Fisher, U.S.A.) spectrometry. The thermal analysis measurements were carried out by differential scanning calorimetry (DSC, DSC1, Mettler Toledo, CH). Samples were heated to 400 °C at a heating rate of 10 °C/min. The samples were all cut from the core of the scaffolds for avoiding any additional variation due to differences in surface and core crystalline structure. The crystallinity of the composites could be calculated using the function expressed in Equation (1):

$$X_c = \frac{\Delta H_m - \Delta H_c}{\Delta H_f \times W_{PEEK}} \quad (1)$$

Where X_c, ΔH_m and ΔH_c refer to the crystallinity, melting enthalpy and crystal enthalpy of PEEK-based composites, respectively. ΔH_f is the enthalpy of fusion of a 100% crystalline PEEK sample (130 J/g), W_{PEEK} is the mass fraction of PEEK in the composites. Relationship between mass and temperature was determined by thermal gravimetric analysis(TGA). PEEK/HA samples were heated to 800 °C at a ramp rate of 10 °C/min by TGA (DSC3, Mettler Toledo, CH).

2.4 Mechanical testing

To assess the influence of HA content, pore size and printing direction on the mechanical properties of the composite scaffolds, PEEK/HA scaffolds were compressed parallel (X printing direction) and perpendicular (Z printing direction) to the printing substrate direction (Figure.1-b) at a compression speed of 3 mm/min. The fabricated PEEK based scaffolds were named as HA content-compressive direction-pore size. For instance, 40%HA-Z-08 means that the HA content was 40 wt.% and the compressive direction was Z printing direction and a pore size of 0.8 mm. The stress-strain curves were obtained from the load-displacement data to calculate the Young's modulus and the strength. Meanwhile, a high-speed camera was used to record the compressive responses of the composite scaffolds to analyze the deformation mechanism.

2.5 Cell compatibility of 3D-printed PEEK/HA scaffolds

The scaffolds with a diameter of 14 mm were put into 24-well plates. Then, preosteoblast cells (MC3T3-E1, ATCC, Manassas, VA, USA) were seeded onto the scaffolds at a density of 2×10^4 cells per well and cultured in α -MEM (HyClone, USA). The MC3T3-E1 cells were proliferated for 1, 3, and 5 days, at which time incubated in the CCK-8 solution. The optical density was measured at $\lambda = 450$ nm using a microplate reader (RT-6000) to qualitatively evaluate the proliferation. The scaffolds were taken into live/dead staining solution and observed by fluorescence microscope (Olympus Co. Ltd.) to evaluate the cell viability. The cells were fixed with 4% paraformaldehyde solution after 5 days culturing and the cell morphologies were observed using SEM. Alizarin Red S (ARS) staining was used to visualize mineralization ability. MC3T3-E1 were cultured on the disc with the diameter of 14mm at a density of 1×10^5 cells. After incubation with the specimens for 24 hours, the culture medium was changed to the osteogenic inductive medium for 21days induction. The stained samples were immersed in DMSO to measure at $\lambda = 550$ nm using a plate reader (RT-6000).

3. Results

3.1 Micro-structure characteristics of the PEEK/HA scaffold

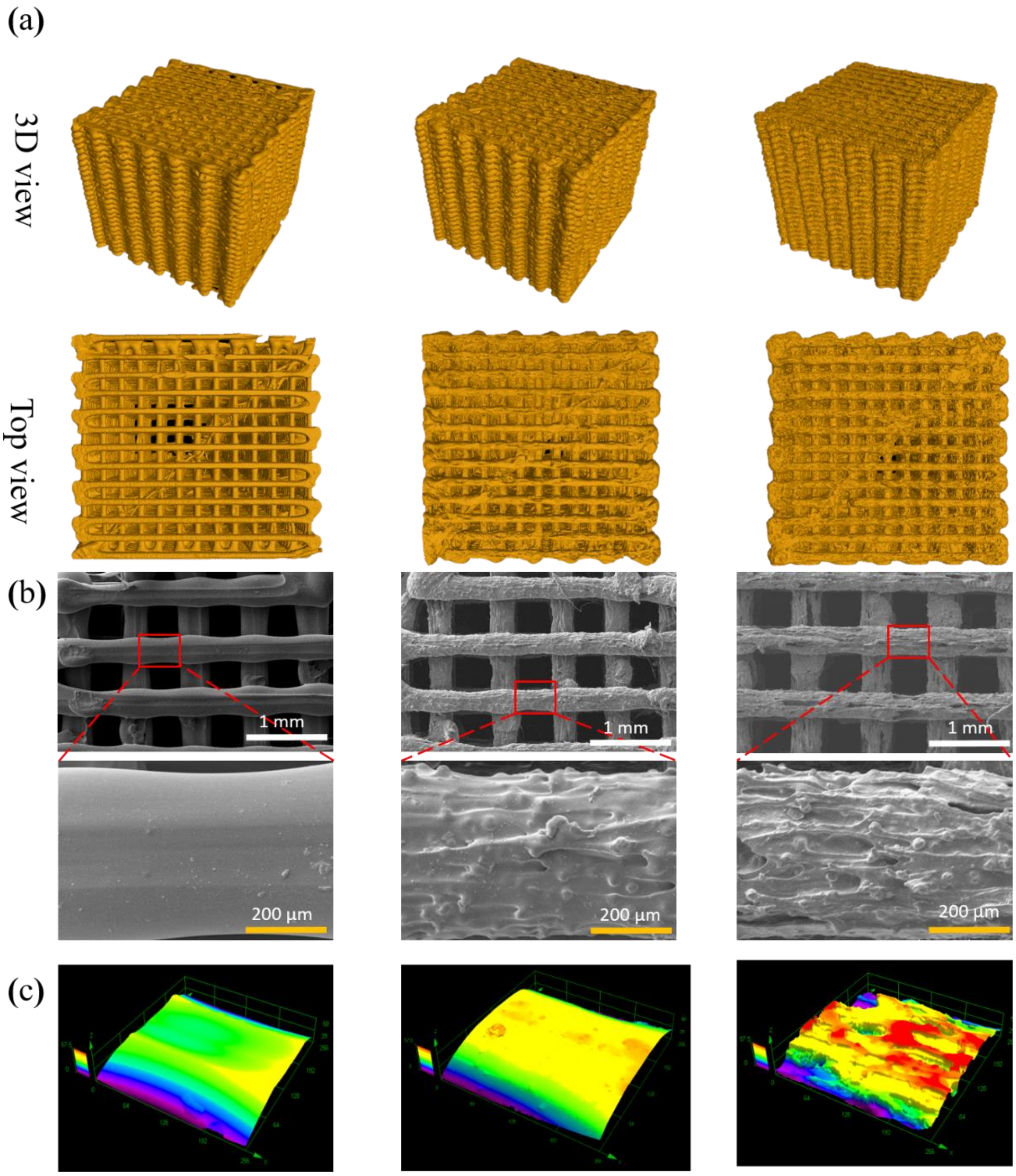

Figure 2. Micro-structure characteristics of the PEEK/HA scaffold samples: (a)Geometry observation by Micro-CT (b) surface morphology by SEM and (c) three-dimensional topography by LSCM. The left column, the middle column and right column represent the pure PEEK, 20%HA and 40%HA scaffolds, respectively. The pore size of three scaffolds is 400μm.

Micro-CT was employed to observe the interconnectivity of the scaffolds as shown in Figure 2-a. It could be seen that no obvious defect on the 3D and top views and the PEEK/HA composite scaffolds exhibited a well interconnectivity. The Figure 2-b showed that the pure PEEK scaffolds exhibited smooth surface, while numerous HA particles and a coarser morphology were observed on the surface of PEEK/HA composites scaffolds. The LSCM results showed that a rougher morphology consisting of peaks and valleys for PEEK/HA composites scaffolds (Figure 2-c), confirming the SEM findings. The pure PEEK scaffold featured a *Ra* of 0.154 ± 0.05 μm, while the *Ra* of the 20%HA and 40%HA scaffolds increased to 0.2486 ± 0.0216 and 2.6 ± 0.318 μm, respectively. Porosity and pore size are positively correlated with the pore size ranging from 0.2 to 2.0 mm as shown in Table1. When the small pore size (0.2~0.8 mm), the porosity of the PEEK/HA scaffolds were higher than that of pure PEEK scaffolds under the same diameter, while the deviation of porosity for the three scaffolds was reduced with the increase of pore size.

Table 1. The porosity of three scaffolds under the different pore size

pore size(mm)	0.2	0.4	0.8	1.2	1.6	2.0
Pure PEEK	47.3±1.20%	59.6±0.88%	72.2±0.79%	74.7±0.37%	77.4±0.35%	84.2±0.73%
20% HA	60.4±0.62%	68.7±1.40%	78.2±0.65%	79.8±0.47%	81.2±1.70%	85.9±1.15%
40% HA	60.9±1.10%	70.2±0.92%	78.4±1.49%	82.3±0.45%	83.7±1.15%	87.8±0.66%

3.2 Thermal behavior of composites

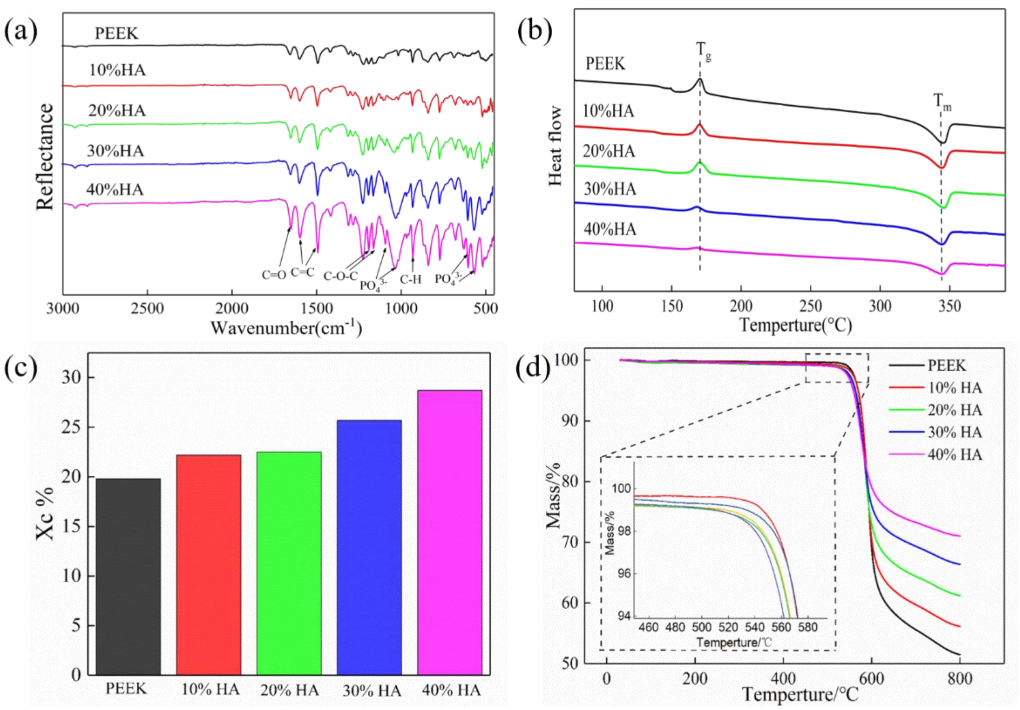

Figure 3. (a) FTIR spectra, (b)DSC curves, (c) crystallinity results and (d)TGA curves of PEEK and PEEK/HA composites.

Figure 3-a showed the FTIR pattern of the pure PEEK and PEEK/HA composites. For the pure PEEK, the peak at 1650 cm^{-1} represented the C=O carbonyl stretching vibration, and the peaks at 1598 cm^{-1} and 1501 cm^{-1} was contributed to the C=C benzene in-plane vibration. The characteristic peaks of PEEK could also be detected in PEEK/HA composites. The peaks of PEEK/HA composites at 1047 cm^{-1} and 570 cm^{-1} are ascribed to the vibration of the PO_4^{3-}, and the increase of HA content resulted the enhancement of PO_4^{3-} peak intensity. The DSC curves showed that a phase transition around 170 °C during the heating process referred to glass transition temperature (T_c) of PEEK (Figure 3b). A sharp endothermic peak around 345 °C corresponded to melting temperature (T_m) of PEEK. The degree of crystallinity of PEEK/HA composites increased with the increase of HA

content (Figure 3-c). When the HA content increased to 40 wt.%, the degree of crystallinity of the composite reached 28.7%. The TGA results show that both PEEK and PEEK/HA composites undergo initial degradation approximately 550 °C (Figure 3d). A sharp drop in mass was observed when the temperature exceeded 560 °C. The initial decomposition temperature shifted to slightly lower temperatures with the increase of the HA content. Meanwhile the residual mass of PEEK/HA composites at 800 ℃ increased with the increase of HA content.

3.3 Mechanical tests

Figure 4-a and Figure 4-b showed the stress-strain curves of scaffolds under compressive process. The stress-strain curves of the scaffolds could be divided into three stages: elastic, plateau and densification, which was consistent with previous investigations[31]. For the PEEK scaffolds compressed along Z printing direction, smooth curves were observed at the plateau stage. However, negligible stress fluctuations were observed at the plateau stage for the scaffolds compressed along X printing direction.

The compressive modulus and the strength were shown as in the Figure 4-c and Figure 4-d. The Young's modulus of the pure PEEK scaffolds compressed along the Z and X printing direction decreased from 371MPa to 102.9 MPa and from the 545.8MPa to 66.3MPa as the pore size increased from 0.2 mm to 2 mm. Compressive strength along the Z compressive direction was higher than that of scaffold along X direction for the scaffolds with the same pore size. The compressive strength of scaffolds can be tuned in the range of 35.2 MPa to 2.2 MPa.

The compressive responses of the 3D-printed scaffolds were shown in Figure 4-e and Figure 4-f. When the scaffolds were compressed along the Z printing direction, the struts of square units were horizontal to loading plate. The gap between layers of scaffolds gradually decreases and then buckling deformation occurred. With the increase of the pore size, the strain corresponding the beginning of the buckling deformation decreases. When the scaffolds were compressed along the X printing direction, the buckling deformation and collapse occurred layer-by-layer, resulting the crush bands (shown by the yellow dotted lines). The crush bands gradually accumulated and the scaffolds were finally compressed into nearly compacted solids.

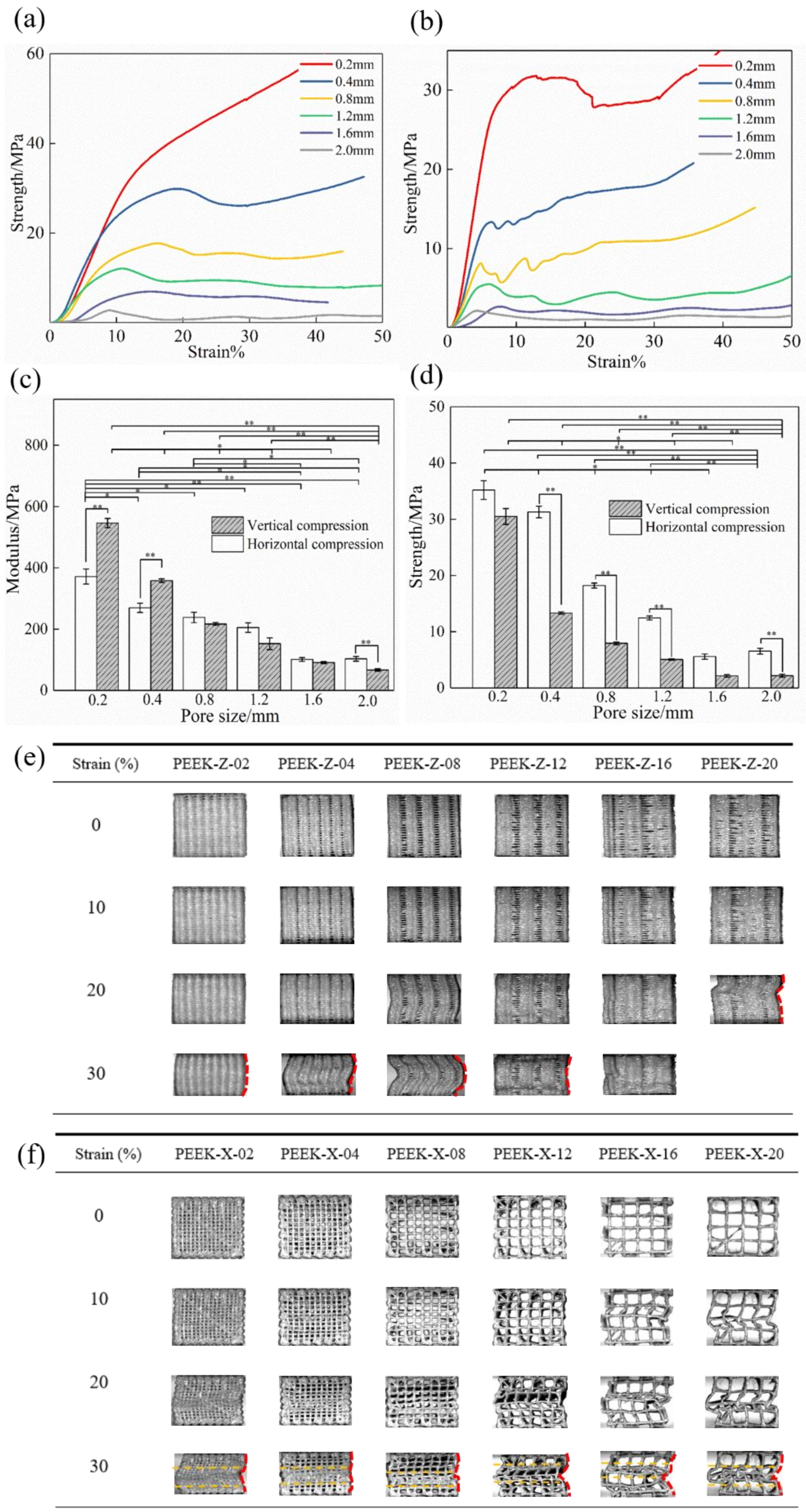

Figure 4. The stress -strain curves of pure PEEK scaffolds compressed along Z (a) and X (b) printing direction. The modulus (c) and strength (d) results of the pure PEEK scaffolds with different pore sizes. The compressive responses of the pure PEEK composite scaffolds compressed along Z (e) and X (f) printing direction.

The mechanical properties of the composite scaffolds with 20 wt.% and 40 wt.% HA content were evaluated. Taking composites scaffold with 40 wt.% HA content as an illustration, the stress-strain curves of PEEK/HA composite scaffolds were shown in Figure 5-a and Figure 5-b. The additive of HA particle reduced toughness of the scaffolds and the stress-strain curves of the composite scaffolds showed a breakage stage instead of plateau and densification after the elastic stage.

The compressive modulus and the strength were shown as in the Figure 5-c and Figure 5-d. Compared with mechanical properties along the X printing direction, the composites scaffold exhibits a higher Young's modulus and a lower compressive strength along the Z printing direction. As the pore size increased from 0.2 mm to 2 mm, the value of Young's modulus along the Z and X printing direction decreased from 374.7 MPa to 112.0 MPa and from 624.7 MPa to 124.2 MPa respectively.

Figure5-e and Figure5-f showed the compressive responses of the PEEK/HA composite scaffolds. The 40%HA-Z-02 and 40%HA-Z-04 scaffolds exhibited a brittle fracture as the strain was > 30%. The larger pore size and porosity reduced the strain corresponding the beginning of brittle fracture. The brittle fracture of 40%HA-Z-12, 40%HA-Z-16 and 40%HA-Z-20 occurred when the strain reached 20%. As the scaffolds were compressed along X printing direction, the struts of the scaffolds were collapsed layer by layer when pore size was <1.6 mm, complied with crush bands accumulation and numerous brittle cracks. 40%HA-X-16 and 40%HA-X-20 scaffold was crushed almost without any deformation when the strain was >10%.

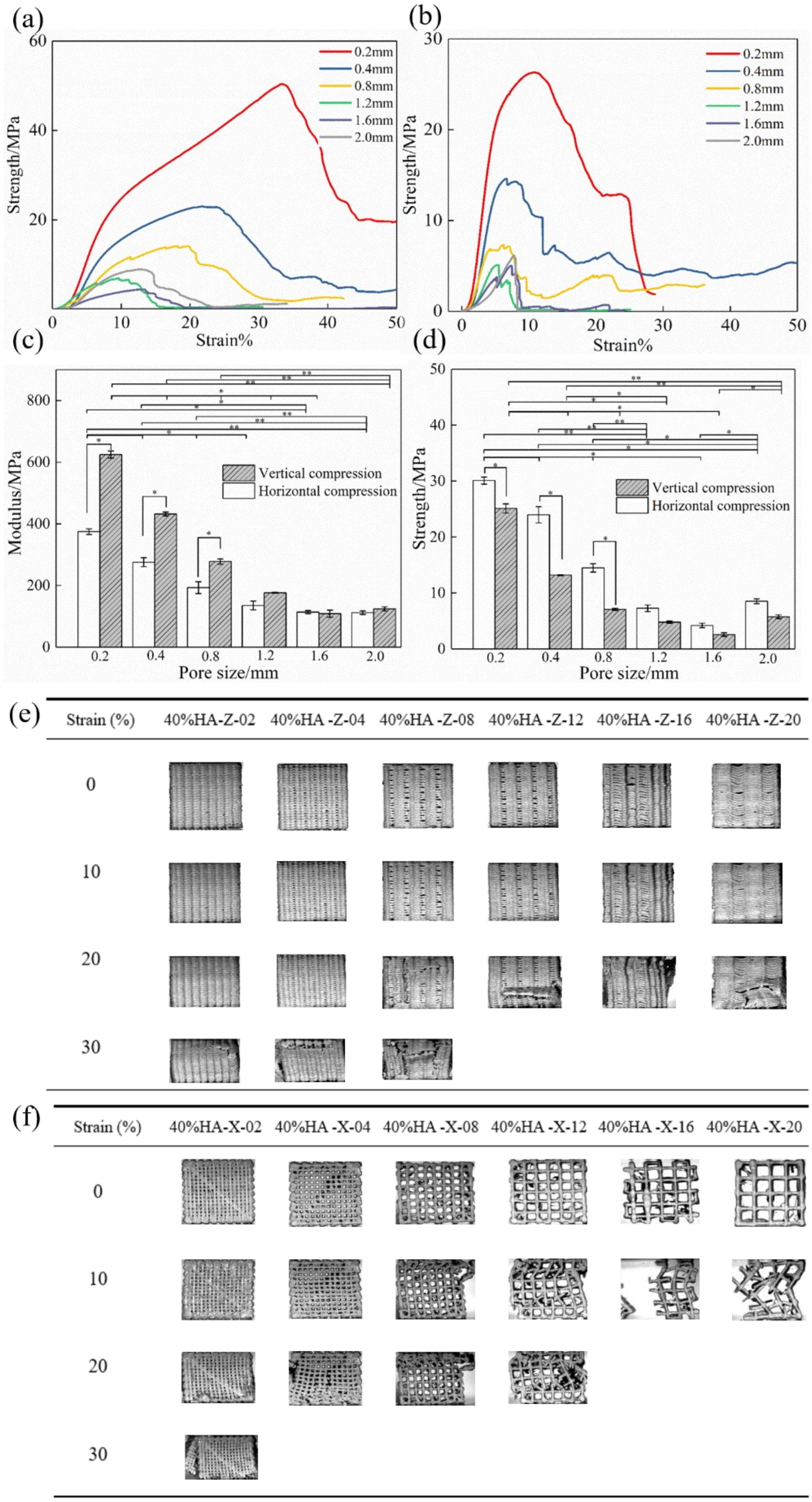

Figure 5. The stress-strain curves of PEEK/HA scaffolds with 40 wt.% HA compressed along Z (a) and X (b) printing direction. The modulus (c) and strength (d) results of the scaffolds with different pore sizes. The compressive responses of the PEEK/HA composite scaffolds compressed along Z (e) and X (f) printing direction.

Figure 6. showed the influence of the HA content and pore size on the mechanical properties of the scaffolds. The relations between the increase in pore size and decrease in modulus and strength can be intuitively understood by the response surface. Changes of HA content have different effects on the modulus anisotropy of the scaffold. When scaffolds were compressed along Z printing direction, no significant changes in modulus was found for the scaffolds with the same pore size, while the modulus of scaffolds remarkably increased with the increase of HA content along the X printing direction. The mathematic relationships between mechanical properties and parameter was obtained by polynomial fitting:

$$E_z = 483.7 - 337d + 0.313r + 84.41d^2 - 0.0187r^2 + 0.0865dr \quad (R^2 = 0.9431) \quad (2)$$

$$\sigma_z = 42.5 - 37.2d - 0.32r + 9.8d^2 + 0.003r^2 + 0.0936dr \quad (R^2 = 0.9712) \quad (3)$$

$$E_x = 644.7 - 676.7d + 1.05r + 198.8d^2 - 0.0214r^2 - 0.583dr \quad (R^2 = 0.9712) \quad (5)$$

$$\sigma_x = 34.5 - 42.6d + 0.064r + 13.38d^2 - 0.001r^2 + 0.0875dr \quad (R^2 = 0.8996) \quad (5)$$

Where E_z and σ_z are the Young's modulus and strength compressed along Z printing direction. The E_x and σ_x are the Young's modulus and strength compressed along X printing direction. d is the pore size and r is the HA content.

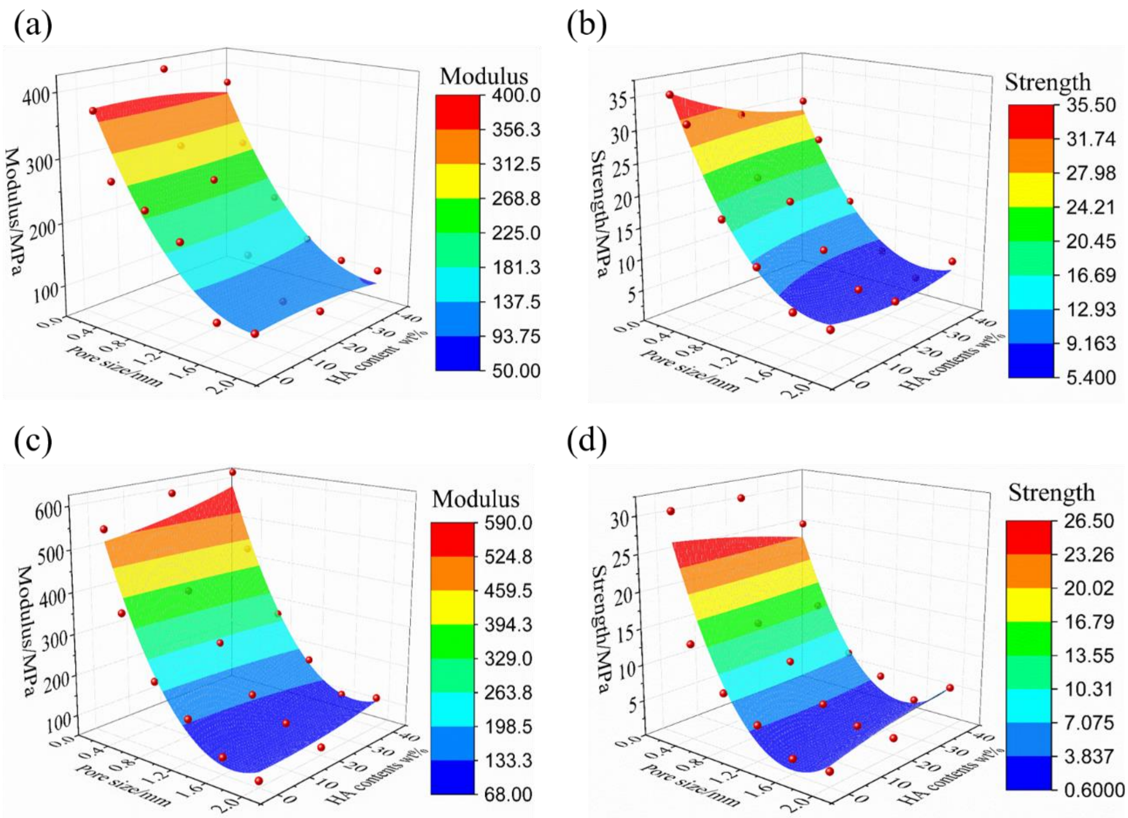

Figure 6. The modulus and strength varied with pore size and HA content: (a) modulus and (b) strength compressed along Z printing direction, (c) modulus and (d) strength compressed along X printing direction.

3.4 Cell compatibility of 3D-printed PEEK/HA scaffolds

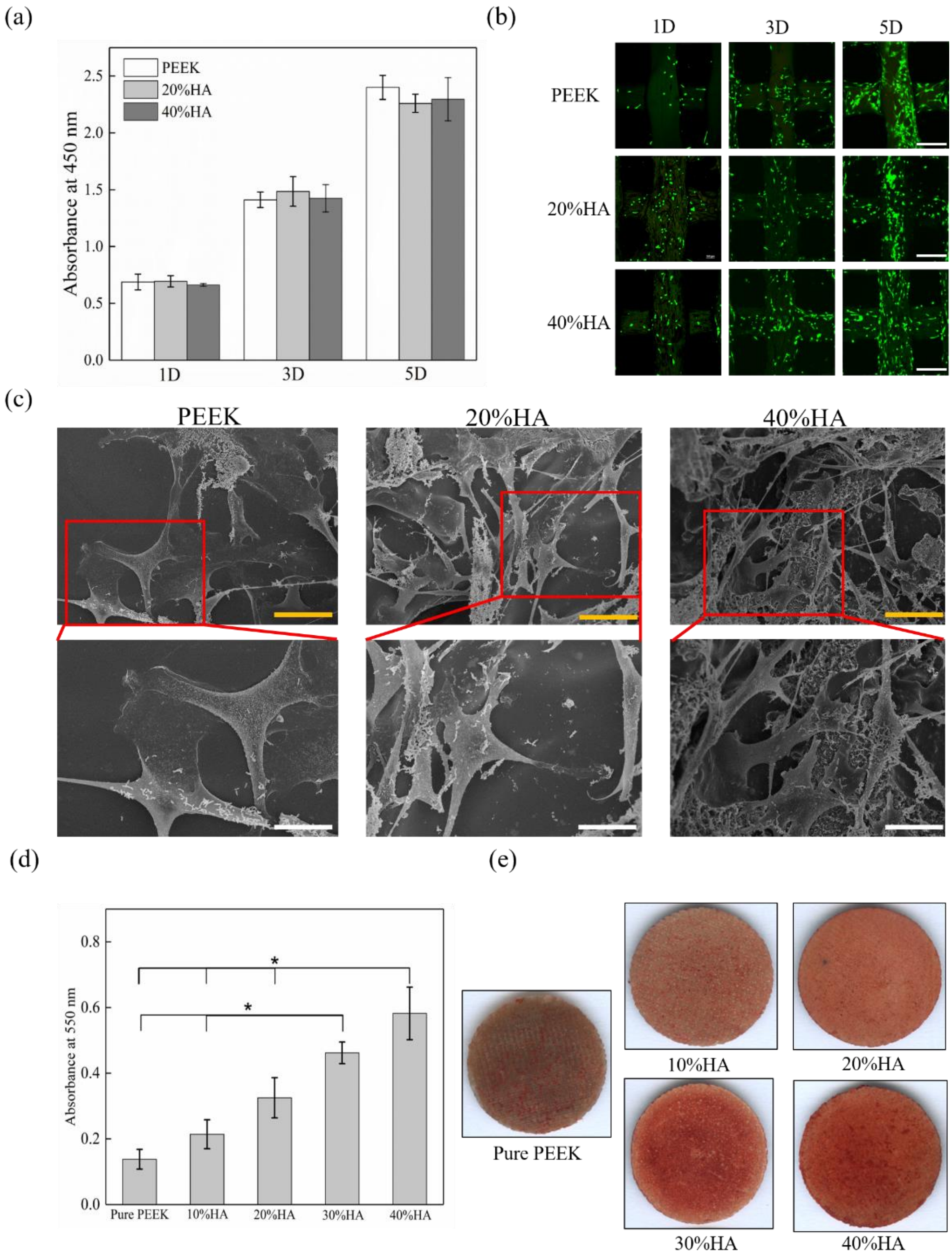

Figure 7. Proliferation, viability, morphology and mineralization of MC3T3-E1 on PEEK/HA scaffolds. (a) Proliferation of MC3T3-E1cell cultured on the scaffolds. (b) viability of MC3T3-E1 cultured for 1, 3, 5 days on the scaffolds. The white bar represented 400 μm. (c) SEM results of adhering MC3T3-E1cultured on the scaffolds for 5 days. The yellow bar represents 50 μm, and the white bar represents 20 μm. (d) quantitative analysis of the alizarin red staining. (e) alizarin red staining of samples with different HA content.

The proliferation of MC3T3-E1 cells on the scaffolds was reflected by OD values as shown in Figure7-a. The OD values of cells on the scaffolds exhibited a persistent increasing proliferation tendency from day 1 to day 7, indicating that both PEEK and PEEK/HA scaffolds exhibited good cytocompatibility. There is no significant difference in the OD values between PEEK and PEEK/HA under the same culture time. Figure7-b displayed that live cells were bright green and elongated filopodia on the scaffolds. A higher number of cells were found on the scaffold with the increase of culture time. Figure7-c showed the morphology of MC3T3-E1 cells on the scaffolds after 5 days of culture and a morphology with an expanded polygonal shape was observed. It could observed that cells on scaffolds with 40 wt.% HA content showed more filopodia than that of cells on pure PEEK scaffold. The mineralization ability of cells was visualized after 21 days of induction as shown in Figure7-d and Figure7-e. Limited calcium nodule was observed on the pure PEEK sample, while obvious calcium deposition was formed on the PEEK/HA scaffolds. The OD values were enhanced with the increase of HA content.

4. Discussion

PEEK, as a polymeric material, was widely used in orthopedic clinics owning to its good biocompatibility and satisfactory mechanical properties. But the biological inertness of PEEK limited its applications for bone repairing. In this study, to enhance the bioactivity and osseointegration ability of PEEK, PEEK/HA composites was prepared by incorporating HA particles into PEEK and the PEEK/HA scaffolds were manufactured via FFF-3D printing technology. Afterwards, the Micro-structure characteristics, thermal behavior, mechanical properties and the biological compatibility of the scaffolds were systematic evaluated.

The printed scaffolds exhibited interconnected structure and the HA content reached up to 40 wt. %. The SEM results for the scaffolds surfaces indicated that the HA particles were not completely embedded in the PEEK matrix but evenly distributed on the surfaces of the composites. The surface roughness and morphology play a critical role in the cell responses for tissue engineering material[32]. Han[33] et al. fabricated the PEEK and PEEK/CF composites samples and found that special printing structures caused by FFF-3D printing process exhibited higher cell densities than the samples being polished and sandblasted process. In this study, the LSCM results showed that the Ra of composite scaffolds with 40 wt. % HA increased to 2.6 ± 0.318 μm. Although PEEK/HA scaffolds had no significant effect on cell proliferation (Figure7-a), more filopodia of cells on PEEK/HA scaffolds indicate that addition of HA particles and micro-structured surface could promote cell attachment and spread, which approved by previous study[34]. The thermal properties of the PEEK scaffold material were measured. For the PEEK/HA composites, because HA particles provided heterogeneous crystallization nucleation points and reducing the nucleation barrier of PEEK in the crystallization process, the degree of crystallinity of composites increased with the increase of HA content. Previous studies[35, 36] had demonstrated that the crystallinity of PEEK could be adjusted by controlling the ambient temperature of FFF 3D printing process. Meanwhile, the increase of crystallinity would reduce the breaking elongation and toughness.

The appropriate mechanical performance could remain the geometric characteristics of the porous scaffold and provide a stress stimulation for the ingrowth of the bone tissue under physiological loading conditions[28]. Meanwhile, the mechanical anisotropy of the porous structure fabricated by 3D printing process directly determines the applications site and stress transmission *in vivo*. However, there was no systematic studies on the mechanical properties and the anisotropy of the FFF printed PEEK/HA scaffolds reported. Results showed that the increase of pore size could reduce the compressive modulus attributed to the increase of the porosity[12]. When the pore size increased to 2.0 mm, the modulus and the strength of the scaffolds dropped below 120 MPa and 9 MPa, respectively. The scaffolds compressed along Z printing direction exhibited higher compressive strength and lower modulus compared with those of the scaffolds compressed along X printing direction. The different loading state of the micro-rods inside the scaffolds was the main reason to the differences of mechanical properties. For the scaffolds compressed along X printing direction, the micro-rods are horizontal to the loading direction and directly bear the compressive loading until bucking deformation. For the scaffolds compressed along Z printing direction, the micro-rods are perpendicular to the loading direction and the interlayer gaps provides space for the bending deformation of the micro-rod, which leads to a lower modulus compared to that of X printing direction. Meanwhile, the higher effective bearing area along Z printing direction contributed to a better compressive strength. The compressive response of pure PEEK scaffolds was mainly plastic deformation, indicating its excellent ductility. The cracks and brittle fractures in the compressive response of PEEK/HA composites demonstrated that the addition of HA particles can significantly reduce the toughness. When the HA content range from 0 to 40 wt. %, the crystallinity increased from 19.8% to 28.7%. The increase of crystallinity and poor interfacial strength between the PEEK matrix and HA particles finally caused toughness decrease of the PEEK/HA composites[35, 37, 38].

The 3D surface representation of the mechanical properties changing with pore size and HA content was investigated and the mathematical relationship among mechanical properties, geometric structure and material components was further established by polynomial fitting. With the porosity of scaffold decreased from about 55% to 85% (Table 1), the Young's modulus and the strength decreased gradually ranging from 624.7-50.6 MPa and 35.2-2.2 MPa, respectively. The adjustable range of the strength and modulus similar to the variation range of the natural trabecular bone (strength: 2–17 MPa, modulus: 344–3230 MPa) [39, 40]. However, the scaffolds exhibited higher Young's modulus and lower compressive strength along Z printing direction. Meanwhile, the addition of HA particle led the decrease of the toughness. In clinical application, the appropriate porosity, printing direction and HA content of the scaffolds should be selected and designed according to the actual biomechanical environment for mechanical stability. The developed mapping relationship could be used in adjusting the mechanical properties of the porous structure to match the properties of the surrounding native bone. The printed scaffolds could be used in low-load-bearing sites to enhance the integration with surrounding bone tissues. The mechanical bionics of the scaffolds would be realized by balancing the mechanical mismatch between the PEEK-based implant with natural bone.

Furthermore, the proliferation, attachment and mineralization ability of MC3T3-E1 cells on the printed scaffolds were fully examined to study the cytocompatibility of the scaffolds. In this study, a pore size of 400 μm was chosen for the scaffold, which has been reported in the literature to be associated with excellent bone ingrowth, vascularization and permeability[41, 42]. The CCK-8 assay results indicated that both the pure PEEK and PEEK/HA scaffolds showed good cytocompatibility and the addition of HA particles had no significant effect on the proliferation the MC3T3-E1 cells. However, Deng et al.[43] and Swaminathan et al.[44] reported that PEEK/HA composites with nanoscale HA particles had a significantly positive influence on cells proliferation. The difference of cells proliferation could be explained that bigger superficial area and nanoscale roughness caused by nanoscale HA particles may exhibit better bioactivity. The obvious spreading of cells on the struts of scaffolds demonstrated that both pure PEEK and PEEK/HA scaffolds provided a suitable biological microenvironment for cell adhesion[15, 45]. Specially, the cells on PEEK/HA scaffolds with 40 wt. % HA content showed more filopodia than that of the cells on pure PEEK scaffolds, demonstrating the better cell adhesion on the PEEK/HA composites. The results of alizarin red staining showed that the addition of HA can significantly increase the mineralization ability of cells on PEEK/HA scaffolds surface, similar to previous studies[46, 47]. But the excessive HA content would reduce the strength and toughness, thus the HA content should be selected to balance the bioactivity and mechanical properties of PEEK/HA scaffolds.

Some limitations of this work must also be recognized. Only the mechanical behaviors of scaffolds with tetragonal structures were evaluated, more bionic architectures, such as dodecahedron, spiral structure, need to be addressed and evaluated for more thorough investigation in the future. Additionally, the mechanical behaviors of the scaffolds were studied under static loading condition. However, the fatigue behaviors of the 3D-printed scaffolds should also be evaluated. Cell experiments *in vitro* was employed to assess the biocompatibility of the scaffolds, but the results cannot fully represent the growth situation of native bone tissue *in vivo*. Therefore, tests under realistic physiological environments such as the animal experiments should be carried out in the future.

5. Conclusion

In this study, the 3D-printed PEEK/HA composites scaffolds with various lever of HA content and pore sizes were fabricated using FFF 3D printing technology. The effects of the pore size, compressive direction and HA content on the mechanical properties were systematically evaluated. The Young's modulus and strength of the PEEK/HA scaffolds could be widely tuned in the range of 624.7-50.6MPa and 35.2-2.2 MPa respectively by increasing the pore size from 0.2 mm to 2.0 mm. The participant of HA was found to significantly enhance the modulus along X printing direction, while the modulus of scaffolds along Z printing direction has no obvious change. The mapping relationship among geometric parameters, HA content and mechanical properties was established, giving more accurate predictions and controllability for the mechanical properties of the scaffolds. The PEEK/HA composites with the micro-structured surface could significantly promote cell attachment and mineralization. Presented study will have a clear impact in the design and mechanical properties control of the PEEK/HA 3D-printed scaffolds for bone tissue engineering.

Acknowledgements

The work was financially supported by the Program of the National Natural Science Foundation of China [51835010], the Key R&D Program of Guangdong Province [2018B090906001], the Project funded by China Postdoctoral Science Foundation [2020M683458], the National Key R&D Program of China [2018YFE0207900], the Fundamental Research Funds for the Central Universities, and "The Youth Innovation Team of Shaanxi Universities."

CL Would like to acknowledge the support of European Union via H2020-MSCA-RISE program(BAMOS project, grant no: 734156) and Engineering and Physical Science Research Council (EPSRC) via DTP CASE programme (Grant No: EP/T517793/1).

Reference

[1] C. Wang, Q.L. Zhao, M. Wang, Cryogenic 3D printing for producing hierarchical porous and rhBMP-2loaded Ca-P/PLLA nanocomposite scaffolds for bone tissue engineering, Biofabrication 9(2) (2017) 12.

[2] L. Wang, J.F. Kang, C.N. Sun, D.C. Li, Y. Cao, Z.M. Jin, Mapping porous microstructures to yield desired mechanical properties for application in 3D printed bone scaffolds and orthopaedic implants, Mater. Des. 133 (2017) 62-68.

[3] N. Sears, P. Dhavalikar, M. Whitely, E. Cosgriff-Hernandez, Fabrication of biomimetic bone grafts with multi-material 3D printing, Biofabrication 9(2) (2017) 11.

[4] S. Ghouse, N. Reznikov, O.R. Boughton, S. Babu, K.C.G. Ng, G. Blunn, et al., The design and in vivo testing of a locally stiffness-matched porous scaffold, Appl. Mater. Today 15 (2019) 377-388.

[5] C.J. Shuai, Y. Cheng, W.J. Yang, P. Feng, Y.W. Yang, C.X. He, et al., Magnetically actuated bone scaffold: Microstructure, cell response and osteogenesis, Compos. Pt. B-Eng. 192 (2020) 11.

[6] M.R. Zhou, J.F. Hou, G. Zhang, C. Luo, Y.Y. Zeng, S. Mou, et al., Tuning the mechanics of 3D-printed scaffolds by crystal lattice-like structural design for breast tissue engineering, Biofabrication 12(1) (2020) 17.

[7] H.M.A. Kolken, S. Janbaz, S.M.A. Leeflang, K. Lietaert, H.H. Weinans, A.A. Zadpoor, Rationally designed meta-implants: a combination of auxetic and conventional meta-biomaterials, Mater. Horizons 5(1) (2018) 28-35.

[8] S. Limmahakhun, A. Oloyede, K. Sitthiseripratip, Y. Xiao, C. Yan, Stiffness and strength

tailoring of cobalt chromium graded cellular structures for stress-shielding reduction, Mater. Des. 114 (2017) 633-641.

[9] F.S.L. Bobbert, K. Lietaert, A.A. Eftekhari, B. Pouran, S.M. Ahmadi, H. Weinans, et al., Additively manufactured metallic porous biomaterials based on minimal surfaces: A unique combination of topological, mechanical, and mass transport properties, Acta Biomater. 53 (2017) 572-584.

[10] S.M. Ahmadi, R. Hedayati, Y. Li, K. Lietaert, N. Tumer, A. Fatemi, et al., Fatigue performance of additively manufactured meta-biomaterials: The effects of topology and material type, Acta Biomater. 65 (2018) 292-304.

[11] C. Yan, L. Hao, A. Hussein, P. Young, D. Raymont, Advanced lightweight 316L stainless steel cellular lattice structures fabricated via selective laser melting, Mater. Des. 55 (2014) 533-541.

[12] R. Baptista, M. Guedes, Morphological and mechanical characterization of 3D printed PLA scaffolds with controlled porosity for trabecular bone tissue replacement, Materials science & engineering. C, Materials for biological applications 118 (2021) 111528-111528.

[13] S. Chen, W. Chen, Y. Chen, X. Mo, C. Fan, Chondroitin sulfate modified 3D porous electrospun nanofiber scaffolds promote cartilage regeneration, Materials science & engineering. C, Materials for biological applications 118 (2021) 111312-111312.

[14] D. Sridharan, A. Palaniappan, B.N. Blackstone, J.A. Dougherty, N. Kumar, P.B. Seshagiri, et al., In situ differentiation of human-induced pluripotent stem cells into functional cardiomyocytes on a coaxial PCL-gelatin nanofibrous scaffold, Materials science & engineering. C, Materials for biological applications 118 (2021) 111354-111354.

[15] Y. Su, J. He, N. Jiang, H. Zhang, L. Wang, X. Liu, et al., Additively-manufactured poly-ether-ether-ketone (PEEK) lattice scaffolds with uniform microporous architectures for enhanced cellular response and soft tissue adhesion, Mater. Des. 191 (2020).

[16] H. Ahn, R.R. Patel, A.J. Hoyt, A.S.P. Lin, F.B. Torstrick, R.E. Guldberg, et al., Biological evaluation and finite-element modeling of porous poly(para-phenylene) for orthopaedic implants, Acta Biomater. 72 (2018) 352-361.

[17] M.Z. Zhao, H.Y. Li, X.C. Liu, J. Wei, J.G. Ji, S. Yang, et al., Response of Human Osteoblast to n-HA/PEEK-Quantitative Proteomic Study of Bio-effects of Nano-Hydroxyapatite Composite, Sci Rep 6 (2016) 13.

[18] R. Ma, S. Tang, H. Tan, J. Qian, W. Lin, Y. Wang, et al., Preparation, characterization, in vitro bioactivity, and cellular responses to a polyetheretherketone bioactive composite containing nanocalcium silicate for bone repair, ACS applied materials & interfaces 6(15) (2014) 12214-12225.

[19] P. Egan, R. Sinko, P.R. LeDuc, S. Keten, The role of mechanics in biological and bio-inspired systems, Nat. Commun. 6 (2015) 12.

[20] A. Higuchi, Q.D. Ling, Y. Chang, S.T. Hsu, A. Umezawa, Physical Cues of Biomaterials Guide Stem Cell Differentiation Fate, Chem. Rev. 113(5) (2013) 3297-3328.

[21] T.Z. Luo, K. Mohan, P.A. Iglesias, D.N. Robinson, Molecular mechanisms of cellular mechanosensing, Nat. Mater. 12(11) (2013) 1063-1070.

[22] C. Shuai, W. Yang, P. Feng, S. Peng, H. Pan, Accelerated degradation of HAP/PLLA bone scaffold by PGA blending facilitates bioactivity and osteoconductivity, Bioactive Materials 6(2) (2021) 490-502.

[23] A. Barba, Y. Maazouz, A. Diez-Escudero, K. Rappe, M. Espanol, E.B. Montufar, et al., Osteogenesis by foamed and 3D-printed nanostructured calcium phosphate scaffolds: Effect of pore architecture, Acta Biomater. 79 (2018) 135-147.

[24] J.F. Kang, E.C. Dong, D.C. Li, S.P. Dong, C. Zhang, L. Wang, Anisotropy characteristics of microstructures for bone substitutes and porous implants with application of additive manufacturing in orthopaedic, Mater. Des. 191 (2020) 10.

[25] K. Hayashi, M.L. Munar, K. Ishikawa, Effects of macropore size in carbonate apatite honeycomb scaffolds on bone regeneration, Mater. Sci. Eng. C-Mater. Biol. Appl. 111 (2020) 9.

[26] D. Melancon, Z.S. Bagheri, R.B. Johnston, L. Liu, M. Tanzer, D. Pasini, Mechanical characterization of structurally porous biomaterials built via additive manufacturing: experiments, predictive models, and design maps for load-bearing bone replacement implants, Acta Biomater. 63 (2017) 350-368.

[27] K. Hazeli, B.B. Babamiri, J. Indeck, A. Minor, H. Askari, Microstructure-topology relationship effects on the quasi-static and dynamic behavior of additively manufactured lattice structures, Mater. Des. 176 (2019) 21.

[28] X.Y. Liang, J.M. Gao, W.K. Xu, X.L. Wang, Y. Shen, J.Y. Tang, et al., Structural mechanics of 3D-printed poly(lactic acid) scaffolds with tetragonal, hexagonal and wheel-like designs, Biofabrication 11(3) (2019) 22.

[29] F.P.W. Melchels, K. Bertoldi, R. Gabbrielli, A.H. Velders, J. Feijen, D.W. Grijpma, Mathematically defined tissue engineering scaffold architectures prepared by stereolithography, Biomaterials 31(27) (2010) 6909-6916.

[30] A. Bagheri, I. Buj-Corral, M.F. Ballester, M.M. Pastor, F.R. Fernandez, Determination of the Elasticity Modulus of 3D-Printed Octet-Truss Structures for Use in Porous Prosthesis Implants, Materials 11(12) (2018) 16.

[31] Z. Meng, J. He, Z. Cai, F. Wang, J. Zhang, L. Wang, et al., Design and additive manufacturing of flexible polycaprolactone scaffolds with highly-tunable mechanical properties for soft tissue engineering, Mater. Des. 189 (2020).

[32] S. Metwally, S. Ferraris, S. Spriano, Z.J. Krysiak, L. Kaniuk, M.M. Marzec, et al., Surface potential and roughness controlled cell adhesion and collagen formation in electrospun PCL fibers for bone regeneration, Mater. Des. 194 (2020).

[33] X.T. Han, D. Yang, C.C. Yang, S. Spintzyk, L. Scheideler, P. Li, et al., Carbon Fiber Reinforced PEEK Composites Based on 3D-Printing Technology for Orthopedic and Dental Applications, J. Clin. Med. 8(2) (2019) 17.

[34] P. Jiang, Y. Zhang, R. Hu, X. Wang, Y. Lai, G. Rui, et al., Hydroxyapatite-modified micro/nanostructured titania surfaces with different crystalline phases for osteoblast regulation, Bioactive materials 6(4) (2021) 1118-1129.

[35] C.C. Yang, X.Y. Tian, D.C. Li, Y. Cao, F. Zhao, C.Q. Shi, Influence of thermal processing conditions in 3D printing on the crystallinity and mechanical properties of PEEK material, J. Mater. Process. Technol. 248 (2017) 1-7.

[36] A. El Magri, K. El Mabrouk, S. Vaudreuil, H. Chibane, M.E. Touhami, Optimization of printing parameters for improvement of mechanical and thermal performances of 3D printed poly(ether ether ketone) parts, J. Appl. Polym. Sci. 137(37) (2020) 14.

[37] M.S. Abu Bakar, M.H.W. Cheng, S.M. Tang, S.C. Yu, K. Liao, C.T. Tan, et al., Tensile

properties, tension-tension fatigue and biological response of polyetheretherketone-hydroxyapatite composites for load-bearing orthopedic implants, Biomaterials 24(13) (2003) 2245-2250.

[38] E.A.B. Hughes, A. Parkes, R.L. Williams, M.J. Jenkins, L.M. Grover, Formulation of a covalently bonded hydroxyapatite and poly(ether ether ketone) composite, Journal of Tissue Engineering 9 (2018).

[39] V. Martin, I.A. Ribeiro, M.M. Alves, L. Goncalves, R.A. Claudio, L. Grenho, et al., Engineering a multifunctional 3D-printed PLA-collagen-minocycline-nanoHydroxyapatite scaffold with combined antimicrobial and osteogenic effects for bone regeneration, Mater. Sci. Eng. C-Mater. Biol. Appl. 101 (2019) 15-26.

[40] E.F. Morgan, T.M. Keaveny, Dependence of yield strain of human trabecular bone on anatomic site, J. Biomech. 34(5) (2001) 569-577.

[41] T. Yu, H. Gao, T. Liu, Y.D. Huang, C. Wang, Effects of immediately static loading on osteointegration and osteogenesis around 3D-printed porous implant: A histological and biomechanical study, Mater. Sci. Eng. C-Mater. Biol. Appl. 108 (2020) 12.

[42] X.P. Tan, Y.J. Tan, C.S.L. Chow, S.B. Tor, W.Y. Yeong, Metallic powder-bed based 3D printing of cellular scaffolds for orthopaedic implants: A state-of-the-art review on manufacturing, topological design, mechanical properties and biocompatibility, Mater. Sci. Eng. C-Mater. Biol. Appl. 76 (2017) 1328-1343.

[43] Y. Deng, P. Zhou, X.C. Liu, L.X. Wang, X.L. Xiong, Z.H. Tang, et al., Preparation, characterization, cellular response and in vivo osseointegration of polyetheretherketone/nano-hydroxyapatite/carbon fiber ternary biocomposite, Colloid Surf.

B-Biointerfaces 136 (2015) 64-73.

[44] P.D. Swaminathan, M.N. Uddin, P. Wooley, R. Asmatulu, Fabrication and Biological Analysis of Highly Porous PEEK Bionanocomposites Incorporated with Carbon and Hydroxyapatite Nanoparticles for Biological Applications, Molecules 25(16) (2020).

[45] H. Spece, T. Yu, A.W. Law, M. Marcolongo, S.M. Kurtz, 3D printed porous PEEK created via fused filament fabrication for osteoconductive orthopaedic surfaces, J. Mech. Behav. Biomed. Mater. 109 (2020).

[46] R. Ma, D.G. Guo, Evaluating the bioactivity of a hydroxyapatite-incorporated polyetheretherketone biocomposite, J. Orthop. Surg. Res. 14 (2019) 13.

[47] R. Ma, Z.F. Yu, S.C. Tang, Y.K. Pan, J. Wei, T.T. Tang, Osseointegration of nanohydroxyapatite- or nanocalcium silicate-incorporated polyetheretherketone bioactive composites in vivo, Int. J. Nanomed. 11 (2016) 6023-6033.

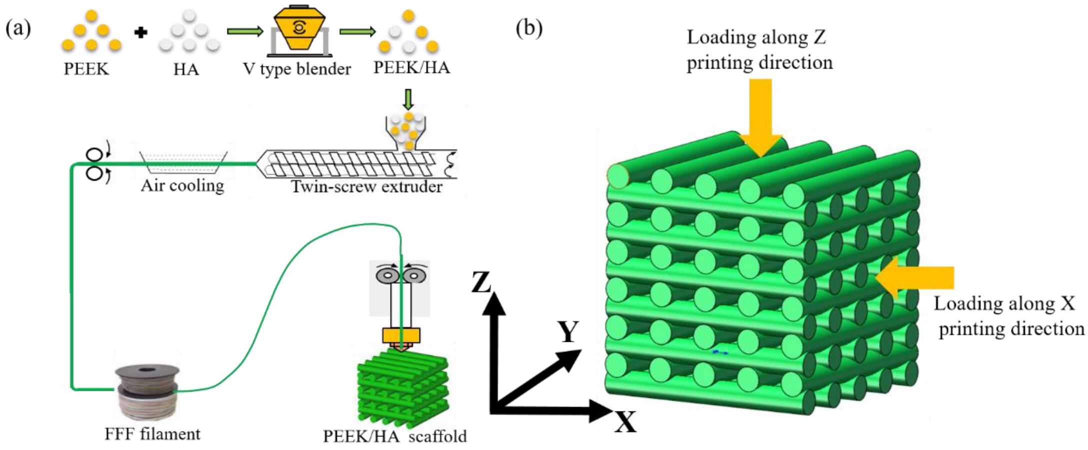

Figure 1. Schematic illustration of the 3D printing process and mechanical properties testing method: (a) preparation of PEEK/HA composites and FFF printing (b) scaffold compressed along Z or X printing direction.

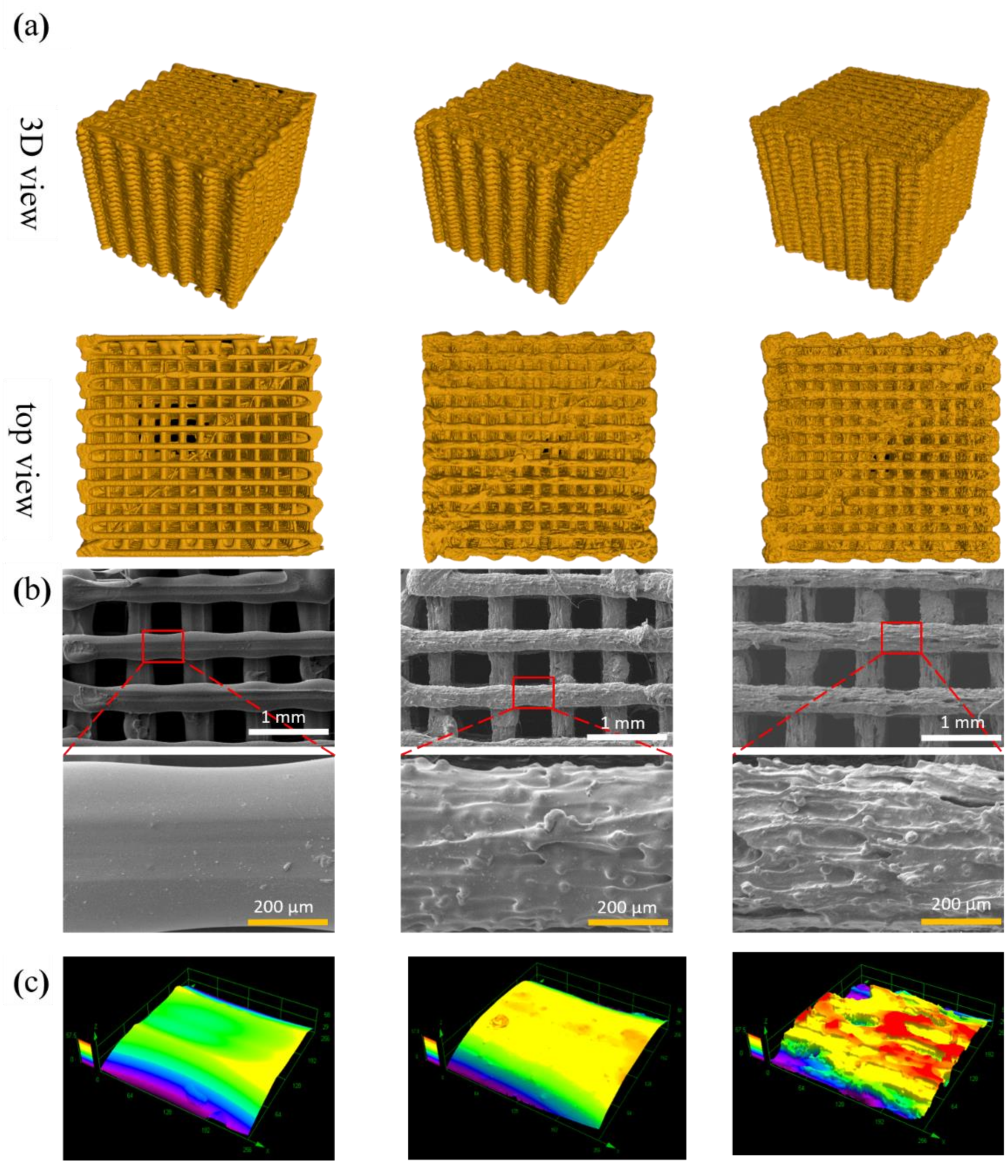

Figure 2. (a) structural characteristics, (b) surface morphology and (c) three-dimensional topography of the scaffolds with pure PEEK, 20 wt.% HA and 40 wt.% HA content.

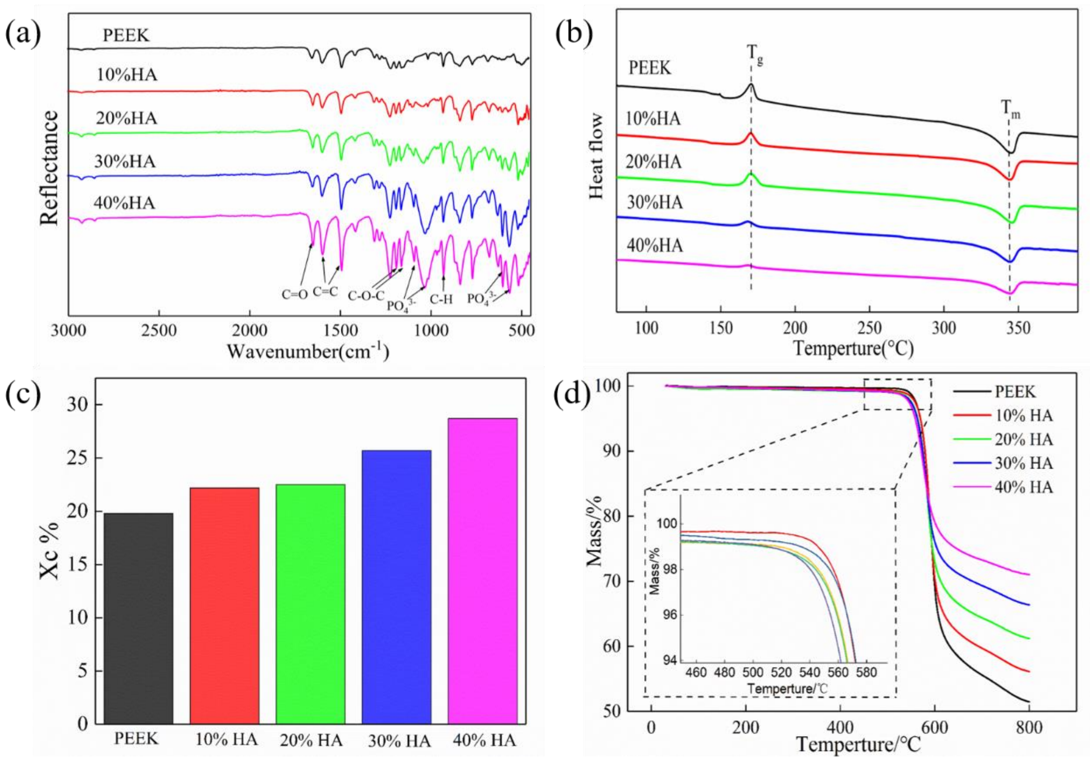

Figure 3. (a) FTIR pattern, (b)DSC results, (c) crystallinity and (d)TGA curves of PEEK and PEEK/HA composites.

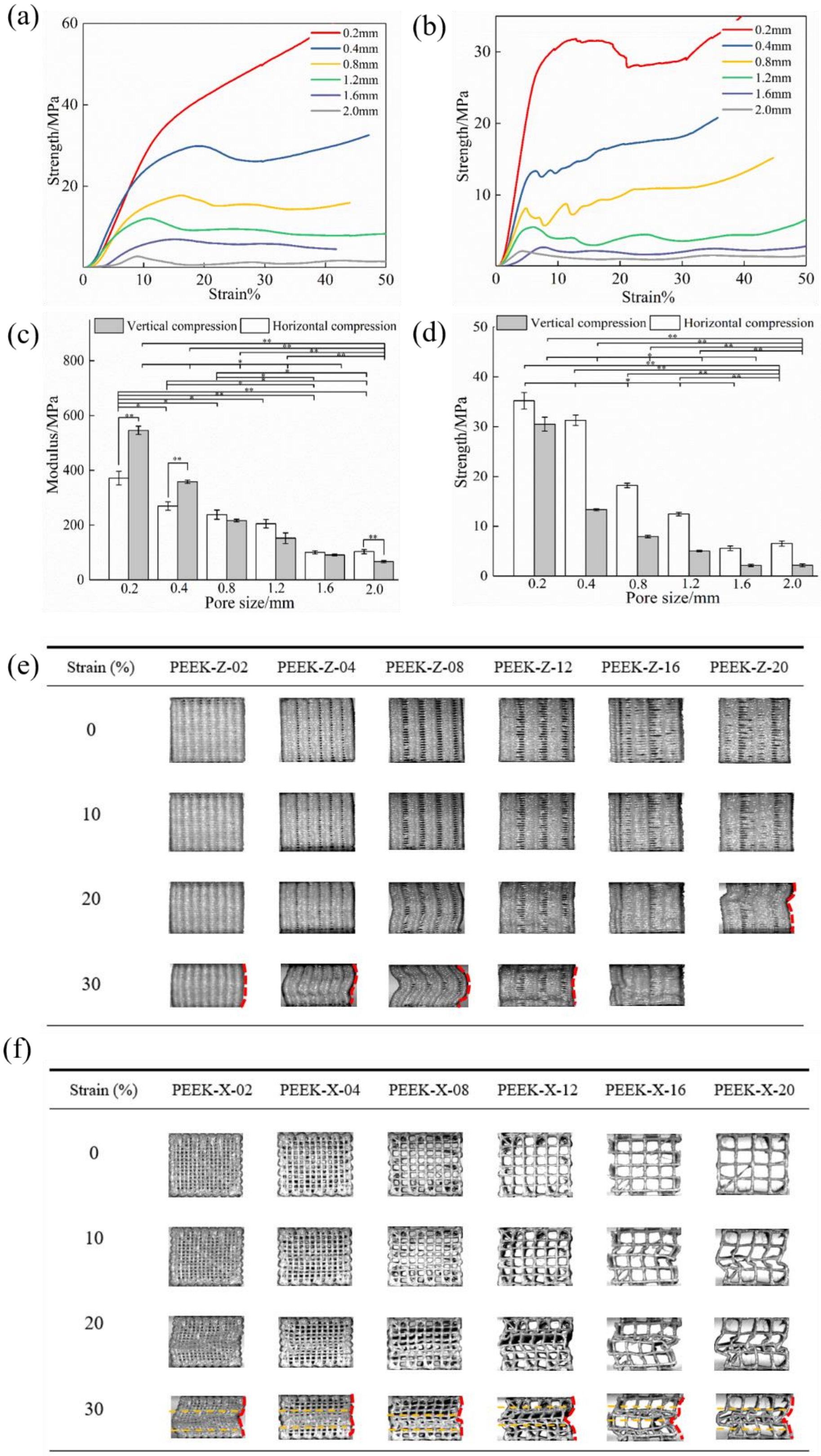

Figure 4. The stress-strain curves of pure PEEK scaffolds compressed along Z (a) and X (b) printing direction. The modulus (c) and strength (d) results of the pure PEEK scaffolds with different pore sizes. The compressive responses of the pure PEEK composite scaffolds compressed along Z (e) and X (f) printing direction.

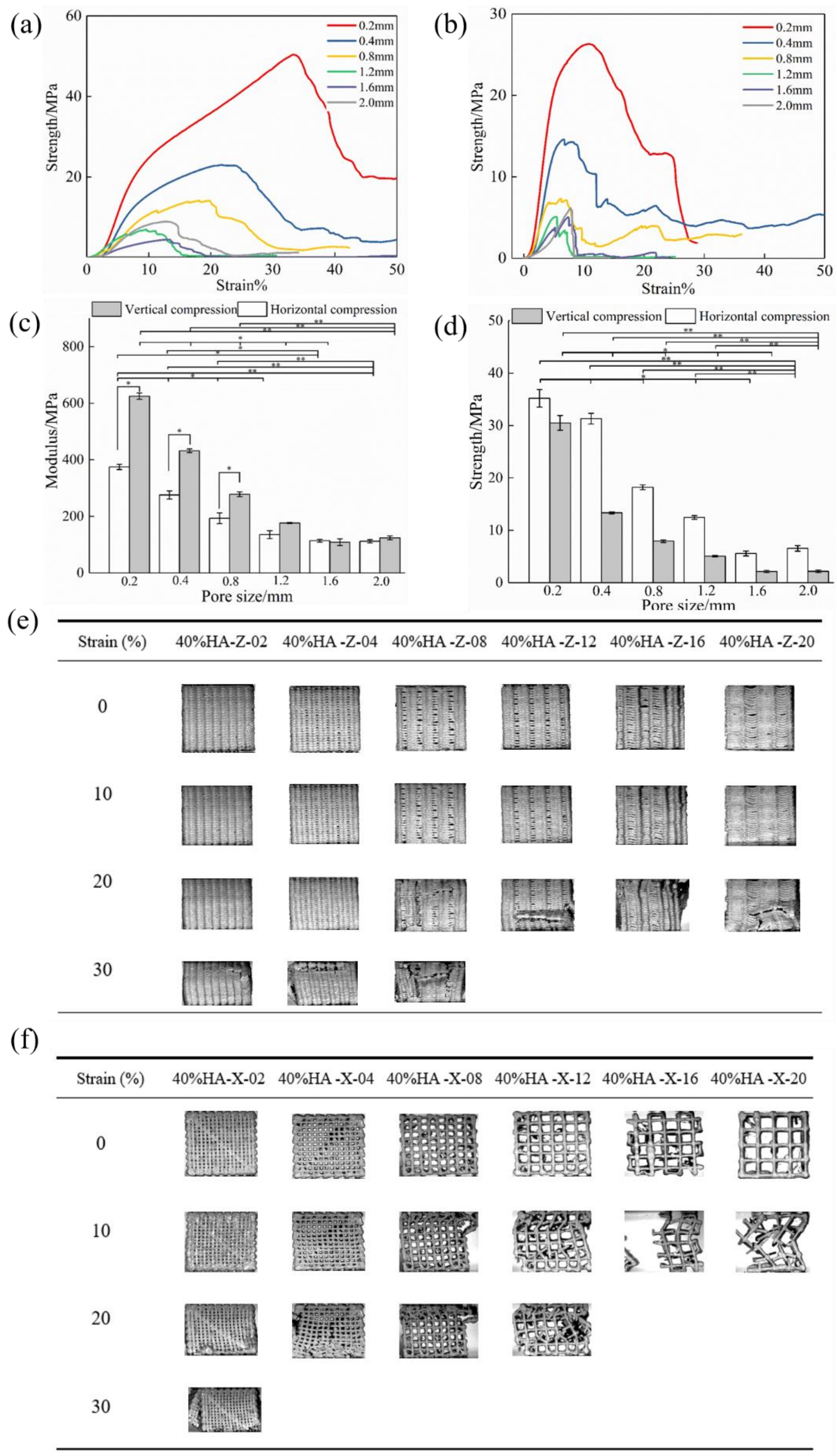

Figure 5. The stress-strain curves of PEEK/HA scaffolds compressed along Z (a) and X (b) printing direction. The modulus (c) and strength (d) results of the scaffolds with different pore sizes. The compressive responses of the PEEK/HA composite scaffolds compressed along Z (e) and X (f) printing direction.

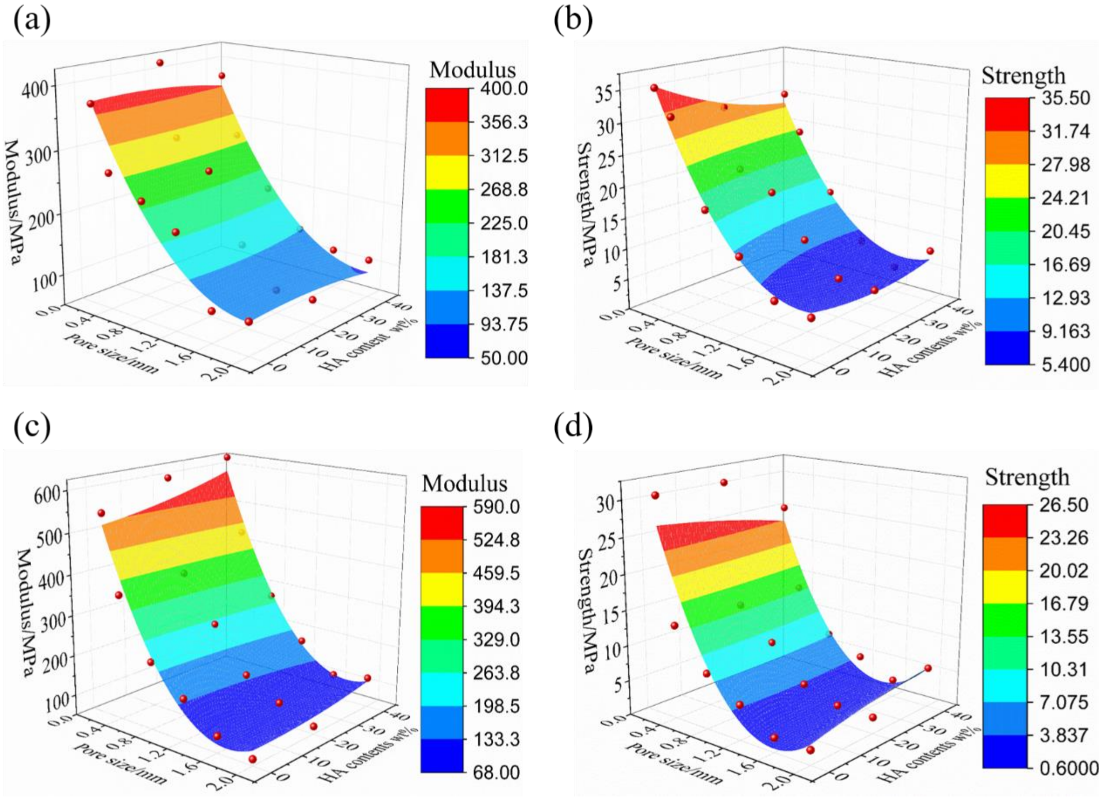

Figure 6. The modulus and strength varied with pore size and HA content: (a) modulus and (b) strength compressed along Z printing direction, (c) modulus and (d) strength compressed along X printing direction.

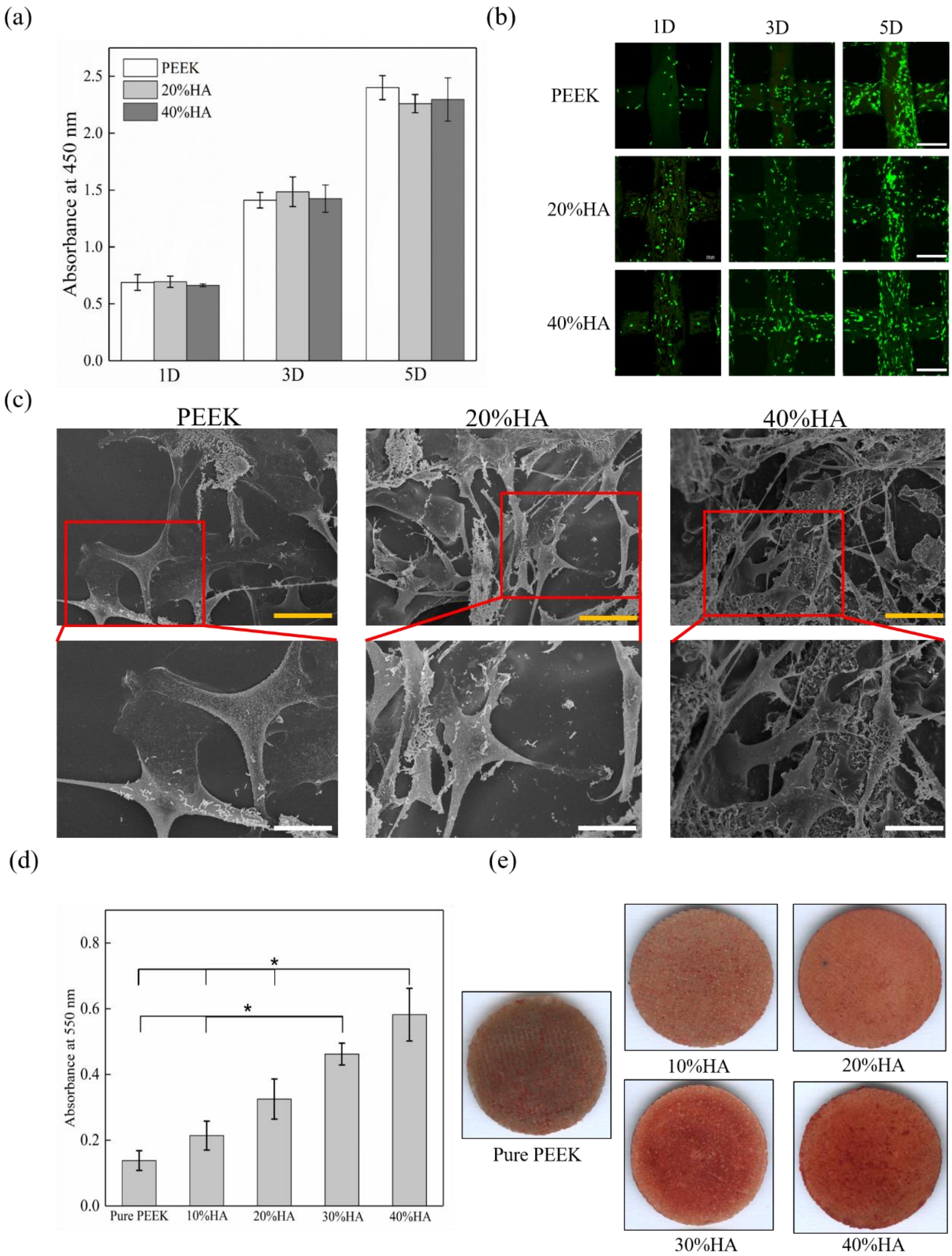

Fig 7. Proliferation, viability, morphology and mineralization of MC3T3-E1 on PEEK/HA scaffolds. (a) Proliferation of MC3T3-E1cell cultured on the scaffolds. (b) viability of MC3T3-E1 cultured for 1, 3, 5 days on the scaffolds. The white bar represented 400 μm. (c) SEM results of adhering MC3T3-E1cultured on the scaffolds for 5 days. The yellow bar represents 50 μm, and the white bar represents 20 μm. (d) quantitative analysis of the alizarin red staining. (e) alizarin red staining of samples with different HA content.

Table 1. The porosity of the scaffolds with different pore size and HA content

Scaffold/pore size(mm)	0.2	0.4	0.8	1.2	1.6	2.0
Pure PEEK	47.3±1.20%	59.6±0.88%	72.2±0.79%	74.7±0.37%	77.4±0.35%	84.2±0.73%
20% HA	60.4±0.62%	68.7±1.40%	78.2±0.65%	79.8±0.47%	81.2±1.70%	85.9±1.15%
40% HA	60.9±1.10%	70.2±0.92%	78.4±1.49%	82.3±0.45%	83.7±1.15%	87.8±0.66%